JOURNAL OF MATERIALS SCIENCE 27 (1992) 5031–5039

Video-controlled tensile testing of polymers and metals beyond the necking point

C. G'SELL, J.M. HIVER, A. DAHOUN, A. SOUAHI
Laboratoire de Métallugie Physique et Science des Matériaux (URA CNRS DO 155), Ecole des Mines de Nancy, Parc de Saurupt, 54042 Nancy Cedex, France

A novel technique has been developed to record the intrinsic plastic behaviour of ductile materials by monitoring the effective strain and the effective stress in the mid-plane of hour-glass-shaped tensile specimens. The method utilizes a computer-aided video extensometer which analyses the sample profile in real time. The effective strain is computed automatically from the minimum diameter, and the effective stress is deduced from the applied load by taking into account the stress triaxiality corresponding to the local radius of curvature of the sample profile. Furthermore, a digital closed-loop system controls the ram speed of the hydraulic tensile testing machine in such a way that the local effective strain rate is maintained at a constant value. It is shown that most polymeric and metallic materials are entitled to be investigated by this method, which gives access in real time to the constitutive plastic equation, up to strains far beyond the necking point. The capabilities of the technique are illustrated and discussed critically, with more details for two polymers of different structures: polyethylene and polycarbonate.

1. Introduction

In many industrial forming processes, the material undergoes a multiaxial deformation far higher than the corresponding necking strain in uniaxial tensile tests. Therefore, for the optimization of these processes, it is essential to make use of reliable equations describing the intrinsic plastic behaviour of a given material element up to very large amounts of deformation. Such equations are commonly expressed in terms of the variation of the effective (generalized) stress versus the effective strain, the effective strain rate and the temperature, σ_{eff} (ε_{eff}, $\dot{\varepsilon}_{eff}$, T). They are necessary for the use of the modern materials forming finite-element codes [1, 2]. Unfortunately, they are generally ill-defined at large strains, because the conventional tensile testing procedures become inefficient as soon as necking occurs. This point is very critical in the case of solid polymers for which tensile inhomogeneities appear for strains as small as 5% [3, 4].

The aim of this paper is to present an original material testing method which was specifically developed for measuring the local stress and strain in a given material element while its local strain rate is held constant by means of a computerized closed-loop control system. In contrast with previous techniques using mechanical clipped-on gauges [5, 6], the present method is enhanced by the application of an image digitizing system and real-time data-processing software, especially designed with a view to achieving fast acquisition and precision control of the stress, strain and strain rate without any mechanical contact with the specimen.

In the experimental section, the basic principles of the method will be presented. Typical results will be subsequently analysed in the case of various materials, with particular attention paid to semi-crystalline polyethylene and amorphous polycarbonate. The intrinsic plastic behaviour of these two reference polymers will be displayed for different strain rates and temperatures. The discussion will be finally devoted to a critical analysis of the limitations and potentialities of the method, which is now routinely applied in this laboratory to the study of several problems of polymer science and engineering, including the prediction of plastic instabilities, the micromechanical investigation of polymeric alloys, and the control of solid-state polymer forming techniques [7–9].

2. Experimental procedure

2.1. Local stresses and strains

In a tensile test-piece subjected to large elongations past the necking point, the deformation of the material becomes highly inhomogeneous along the calibrated portion. Consequently, local values of the tensile stress, strain and strain rate should be defined instead of the overall values (or nominal, or engineering) usually considered for small elongation ratios. The scale at which these local variables are suitably measured depends on the geometry of the sample and on the microstructural deformation mechanisms of the material considered. More specifically, the dimensions of the material element concerned in these measurements should be much smaller than the characteristic

0022–2461

wavelength of the macroscopic strain gradients (necks), but much larger than the microscopic deformation domains (grains, spherulites, fine shear bands etc.).

In the case of the standard ASTM specimens commonly used to test materials in tension, the calibrated portion has a constant cross-section. Subsequently the necks may appear in any place. Furthermore, in the case of flat specimens, they tend to grow obliquely, leading to a complex combination of shear and extensional strains, whose distribution is hardly predictable. It has been shown previously on theoretical and experimental grounds [10, 11] that the use of cylindrical "hour-glass" specimens (Fig. 1) minimizes the above problems because the neck develops uniquely from the centre of the sample, with simpler axisymmetric distributions of the stresses and strains. Although the components of both the stress and strain tensors vary along the tensile axis, z, and along the radial axis, r, it was shown previously, by means of finite-element computations, that the axial variation predominates in the central region. Following this "long wavelength" approximation [12], the "true" local stress in the mid-plane of the specimen is close to the Kirchoff expression

$$\sigma_{zz} = \frac{4F}{\pi D^2} \tag{1}$$

Where D is the minimum diameter of the deformed sample. A suitable triaxiality correction is nevertheless recommended in order to take into account the (small) triaxiality effect associated with the development of the radial and circumferential components of stress when the neck profile takes a marked curvature. On the basis of the Von Mises flow laws, Bridgman [10] has shown that the "effective " stress (equivalent tensile stress for a pure uniaxial field) is approximately obtained by multiplying σ_{zz} by a scalar triaxiality factor, F_T, depending only on the neck geometry

$$\sigma_{eff} = \sigma_{zz} F_T = \sigma_{zz}\left(\frac{1}{[1 + (4R_c/D)] \log[1 + (D/4R_c)]}\right) \tag{2}$$

where R_c is the radius of curvature of the profile in the centre of the neck. Among others [13], the analysis of Bridgman is the most commonly accepted. Its operational validity has been checked for polyethylene samples in previous publications [3, 4, 7].

Concerning the strain field, its average radial component in the mid-plane of the sample is simply related to the local reduction of diameter

$$\varepsilon_{rr} = \log(D/D_0) \tag{3}$$

where D_0 is the minimum diameter of the undeformed specimen. This way of assessing the deformation of the material has three advantages: (i) it concerns the same material plane as for the measurement of the stress, (ii) the state of stress and strain in this plane has the singular property of being nearly uniform for symmetry reasons [10], and (iii) it can be continuously monitored from a simple optical measurement of the narrowest diameter of the developing neck.

In the case when the material is transversally isotropic and deforms at constant volume (these assumptions will be discussed in a later section), the axial component of strain is directly deduced from the radial component by the relation

$$\varepsilon_{zz} = -2\varepsilon_{rr} \tag{4}$$

and, since the stress triaxiality effects in the plane of symmetry are of a second-order amplitude, their influence on the local distribution of strain can be neglected. Consequently, in the following matter, the local effective strain will be expressed to a first approximation by

$$\varepsilon_{eff} = \varepsilon_{zz} = 2\log(D_0/D) \tag{5}$$

Therefore the effective strain rate is locally correlated with the neck shrinkage rate though the relation

$$\dot{\varepsilon}_{eff} = \frac{d\varepsilon_{eff}}{dt} = -\frac{2}{D}\left(\frac{dD}{dt}\right) \tag{6}$$

The problem of performing a tensile test with a locally constant strain rate consists therefore in the appropriate control of the specimen elongation rate in

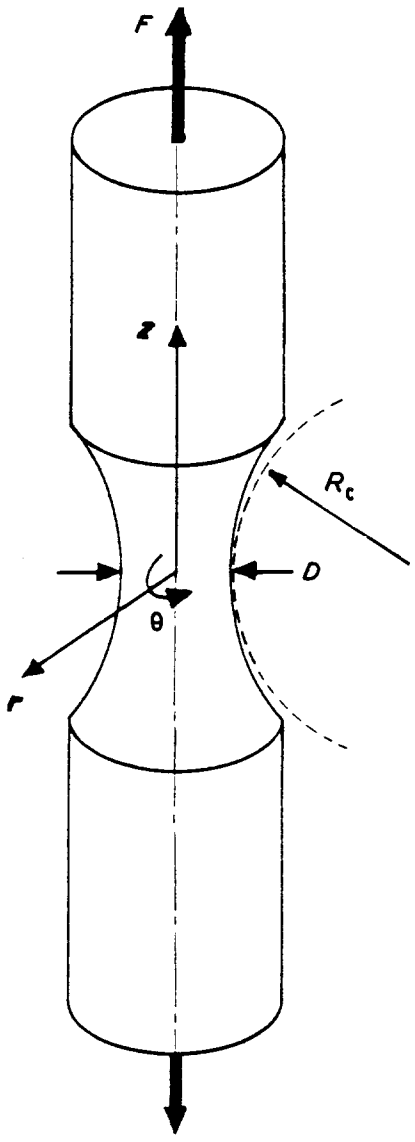

Figure 1 Diagram of the hour-glass-shaped tensile sample.

such a way that the minimum diameter would decrease according to an exponential function as

$$D(t) = D_0 \exp\left(-\frac{\dot{\varepsilon}_{eff}}{2}t\right) \quad (7)$$

In previous work [6], one of us has developed a preliminary technique in which the minimum diameter was measured by the use of a circumferential extensometer, while its appropriate evolution with time was controlled by means of an MTS servo-hydraulic testing machine and an exponential function generator. This system was satisfactory, but the strain control was somewhat jerky due to the friction of the thin cable driving the circumference measurement at the minimum cross-section of the neck. In further experiments, the system was improved by the use of a diametral clip-gauge. Jerkiness was thus suppressed, but the basic problems of mechanical extensometry remained: (i) the installation of the clip-gauge on to the specimen was tedious and risks of slippage were permanent, (ii) the technique was limited to temperatures lower than about 200 °C unless a delicate remote rod-driven measuring system was used, (iii) the clipped-on extensometer impeded the *in situ* observation of defects (cracks, asymmetric shear bands) which may arise in the sample during the test, and (iv) the clipping pressure of the extensometer arms at the contacting points was likely to damage the specimen in the case of very delicate materials.

With regards to the above problems, non-contacting optical extensometry appeared to be very attractive. Its feasibility was founded on previous experiments [3, 4] in which the deformation of tensile samples was determined from their photographic survey. The precision was correct but the *post mortem* processing of strain data from the recorded images was lengthy and made impossible any interactive procedure. Subsequently, the new method described here was developed to analyse optically the current profile of the specimen during the course of a tensile test and to control the local strain rate in real time, up to very large strains far beyond the necking point.

2.2. Experimental apparatus

The system developed for this work is controlled by a fast-processor microcomputer (Compaq 386, 25 MHz) interfaced with a servo-hydraulic tensile testing machine (MTS 810), a video camera, a keyboard and several imaging and plotting displays (Fig. 2).

The opto-electronic equipment is composed of the camera and its digitizing interface which records in real time the specimen profile under load. The camera is a CCD model from I2S (IVC/500). It is equipped with a 200 mm tele-lens mounted on a Nikon bellows to allow focusing at the rather short frontal distance (about 300 mm) between the lens and the specimen. The video interface board is commercially available from Matrox of Dorval, Canada (Ref. MVP-AT). It digitizes the video frame within 40 ms in an array of 512 × 512 pixels. The brightness of each pixel is analysed on a 256-level grey scale.

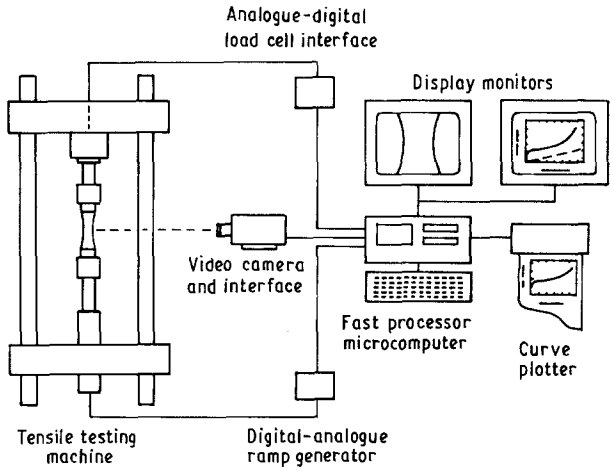

Figure 2 General diagram of the tensile testing system with the computer-aided video extensometer and the true strain-rate control.

The interface of the tensile machine with the microcomputer is of the input/output type. On the one hand, the signal from the load transducer is treated by a 12-bit analogue-to-digital circuit (resolution of 5 N for a typical full scale of ± 10 kN). On the other hand the input signal of the hydraulic actuator is controlled by a specially designed 16-bit digital-to-analogue interface (resolution of 0.6 μm for a typical full scale of ± 20 mm), equipped with a programmable ramp generator with its own clock.

The software (named VideoTension) was designed for computing in real time the effective stress and effective strain from the recorded data. It is also capable of controlling the tensile test at a constant true strain rate. It is composed of interchained subroutines whose flow chart is illustrated in Fig. 3. The user-configurable subroutines were written in compiled Basic language, while all the subroutine which require a very high execution speed (for the processing of the video images in particular) were written in the C programming language.

The initial setting subroutine is run before the tensile test is activated, in order to adjust all the physical and logical parameters of the system: calibration of the load cell and of the actuator, adjustment of the video camera (brightness, contrast and threshold), programming of the ramp generator, identification of the test, choice of the format for the stress–strain curve plotting. Lastly, the program allows the user to mount the tensile specimen in the grips of the MTS machine.

Once the ramp generator is switched on, the Tension Control subroutine supports all functions necessary to (i) acquire the tensile force, F, from the load cell, (ii) measure the geometric variables (D, R_c) from the video interface, (iii) compute and save the effective stress and strain (σ_{eff}, ε_{eff}) by taking into account the Bridgman triaxiality factor, F_T, (iv) adjust the hydraulic ram velocity in such a way that the local strain rate, $\dot{\varepsilon}_{eff}$, remains constant in the mid-plane of the sample, and (v) plot the stress versus strain and the strain versus time curves on the high-resolution monitor of the microcomputer.

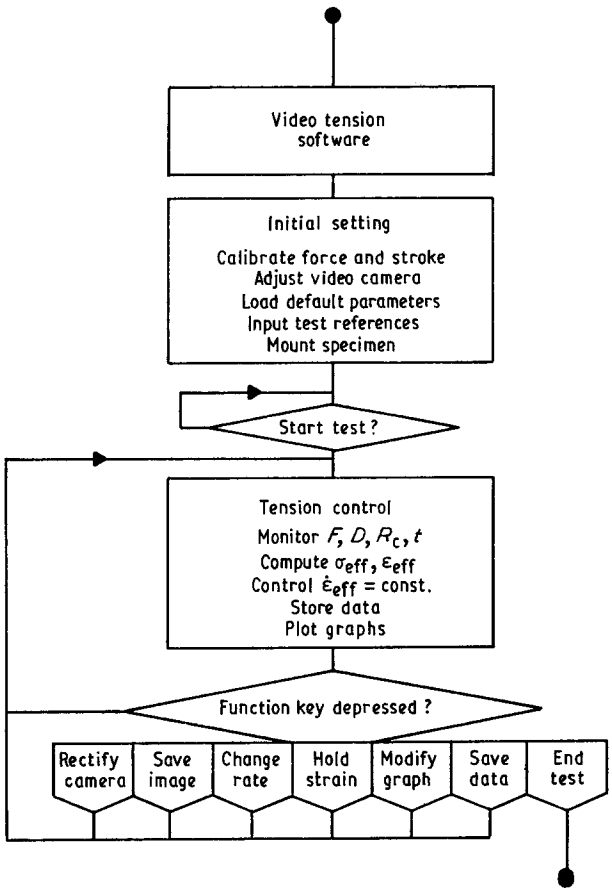

Figure 3 Flow chart of the VideoTension software designed for the control of tensile tests at constant effective strain rate.

The above subroutine was carefully designed in order to optimize the accuracy of the physical measurements (F, D, R_c, t) together with the stability of the strain rate. In this scope, the computing speed was accelerated by the use of an 80387 math-coprocessor, which makes possible the numerical filtering of the acquired data.

The capabilities of this tensile testing system have been analysed during the last four years and permanently upgraded by the introduction of newly available components or peripherals. In addition, a companion software (named DataGraph) was developed for the functional analysis of the stress–strain–strain-rate plots.

This development was based on the following principles:

(i) systematic use of commercial hardware elements as far as they are available at a reasonable cost (only the ramp generator was customized);

(ii) a user-friendly interface adapted to untrained users: the menu-guided software indicates the alternative operations at any step of the test and its Basic language source can be easily modified by a novice programmer;

(iii) flexible adaptation to other types of test with the same hardware elements (different versions of the system will be presented in the discussion section).

3. Results

A wide variety of materials has been tested in tension by means of this apparatus, including polymers (polyethylene, polycarbonate, polyamide 6, poly(oxymethylene,), polystyrene, poly(tetrafluoroethylene), poly(vinylchloride), poly(ether ether ketone), poly(methyl methacrylate), and metals (carbon steel, copper–zinc brass, aluminium alloy). Some characteristics of these materials are listed in Table I. All the specimens were machined on a lathe out of plates or rods, with an original diameter $D_0 = 6$ mm in the mid-plane cross-section, and a radius of curvature $R_c = 20$ mm.

It should be noted that the present method is of particular interest for polymers, since these materials exhibit a very early necking phenomenon, as illustrated by the profiles of Fig. 4 in the case of a high-density polyethylene sample. These profiles were obtained directly from the video camera and stored in a hard disk during a typical tensile experiment at 25°C. The first image represents the central part of the original hour-glass-shaped sample. The others show the formation of the neck and the corresponding evolution of the specimen profile.

Selected stress–strain curves obtained with these materials will be presented below, with particular attention paid to the contrasting cases of the flexible semi-crystalline high-density polyethylene and the glassy amorphous polycarbonate, which better illustrate the capabilities of the testing procedure and which have been investigated extensively in this laboratory [3, 4, 6–9, 15].

3.1. High-density polyethylene

Effective stress–strain curves obtained with the present technique are displayed in Fig. 5 for the polyethylene at room temperature and for four effective strain rates in the range from 5×10^{-5} to 1×10^{-3} s^{-1}. At small strains, the behaviour is inelastic with an initial tangent modulus of about 600 MPa, characteristic of the semi-crystalline structure with rigid crystallites (about 71% by volume, as determined by density measurements) embedded in a rubber-like amorphous polymer. After a period of moderate decrease of the slope, the material experiences a yield phenomenon which corresponds to the knee of the effective stress–strain curves, followed by a long plastic stage with very small strain-hardening. It is widely acknowledged [16, 17] that the plastic yielding of polyethylene is associated with the initiation of glide mechanisms parallel to the chains in the crystalline lamellae which are inclined about 45° with respect to the tensile axis (and which thus undergo the highest resolved shear stress).

It is essential to remark that the effective stress–strain curves of the polyethylene do not exhibit any stress drop at yield, in contrast with the engineering (nominal) curves usually displayed in the literature. In the latter, the engineering stress drop is typically of the order of 40% of the yield stress, this effect being so dramatic that many authors have considered this drop as an intrinsic feature of polymer behaviour. Contrary to the above statement, the continuous increase of the stress in the effective curves presented here proves that the transient drop of the engineering stress for polyethylene is entirely due to geometric and rate effects,

TABLE I List of the materials tested

Symbol	Material	Origin	Treatment[a]	Density ($g\,cm^{-3}$)	(vol %) crystallinity[b]
HDPE	High-density polyethylene	Union Carbide, DFDY 6130, $M_w = 192\,200\ g\,mol^{-1}$	60 °C/24 h	0.965	71
PC	Bisphenol-A polycarbonate	Bayer-Röhm, Makrolon L, $M_w = 28\,800\ g\,mol^{-1}$	110 °C/24h	1.1975	0
PA 6	Polyamide-6	BASF, Ultramid B3	120°C/24h	1.133	33
POM	Poly(oxy methylene)	Commercial rod	120 °C/24 h	1.401	67
PS	Polystyrene, atactic	Westlake Plastics, USA, $M_w = 59\,900\ g\,mol^{-1}$	95 °C/24 h	1.050	0
PTFE	Poly(tetra fluoro ethylene)	Commercial rod	40 °C/24 h	2.149	49
PVC	Poly(vinyl chloride)	Carlew Chemicals, D101 dark grey	As received	1.396	0
PEEK	Poly(ether ether ketone)	Imperial Chemical Industries, 450 G	160 °C/24 h	1.304	29
PMMA	Poly(methyl methacrylate)	Orkem, PD 2774	85 °C/24 h	1.188	0
PP	Polypropylene, isotactic	Atochem, 3050 MN1	120 °C/24 h	0.910	61
Steel	Iron alloy 35 CD 4	Commercial rod	Normalized	7.90	100
Brass	Copper–Zinc alloy	Commercial rod	300 °C/2 h	8.46	100
Al	Aluminium alloy AU 4 G	Commercial rod	As received	2.79	100

[a] Thermal treatment under vacuum (except for brass in air), followed by a very slow cooling.
[b] Index of crystallinity deduced from the measured density and from published values of the crystal and amorphous densities [14].

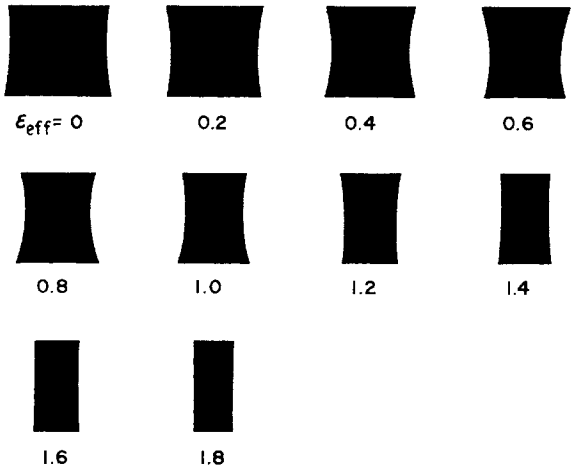

Figure 4 Evolution of the specimen profile under tension in the case of high-density polyethylene at 25 °C.

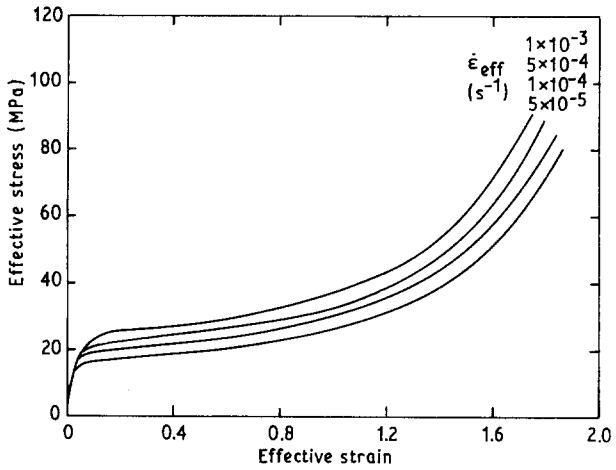

Figure 5 Effective stress–strain curves of high-density polyethylene at 25 °C for various effective strain rates.

namely those associated with the sudden formation of a neck which supports most of the overall elongation.

Once the plastic regime is installed, it continues readily up to very large strains. The originally moderate strain-hardening increases gradually, due to the orientation of polymeric chains in the amorphous parts and to the development of a fibre texture among the crystalline species [17, 18]. However, the curve does not exhibit any discontinuity like the so-called "cold-drawing plateau" often described in the literature from conventional tensile tests and which is merely associated with the propagation of the neck along the specimen. Here, because the effective behaviour is determined locally, the increase of stress characterizes the progressive strain-hardening of the selected material element as its deformation proceeds at a constant strain rate: whatever happens to other parts of the specimen could not influence its evolution (by contrast with the conventional test in which a material element located in the initially necked zone may wait at nearly zero strain rate for a very long time before the remote elements are reached in turn by the necking "wave").

From the remarks above, it is clear that one advantage of this testing technique is to give access to the influence of the effective strain rate directly. This is illustrated in Fig. 5 which shows that, in all the plastic stage, the tensile stress increases by about 20% for a tenfold increase of the strain rate.

Lastly, the method gives access to the determination of the influence of the temperature on the deformation process for a given strain rate (Fig. 6). The tensile behaviour of the polyethylene appears to be very sensitive to temperature, with a 50% reduction of the yield stress between 25 and 70 °C, although the general shape of the curves remains unchanged.

3.2. Polycarbonate

Contrasting with the case of polyethylene, the effective stress–strain curves obtained with polycarbonate at room temperature (Fig. 7) show a definite yield drop at the initiation of the plastic regime. Since the effective stress is still related to the local response of the central material element, the transient stress peak observed

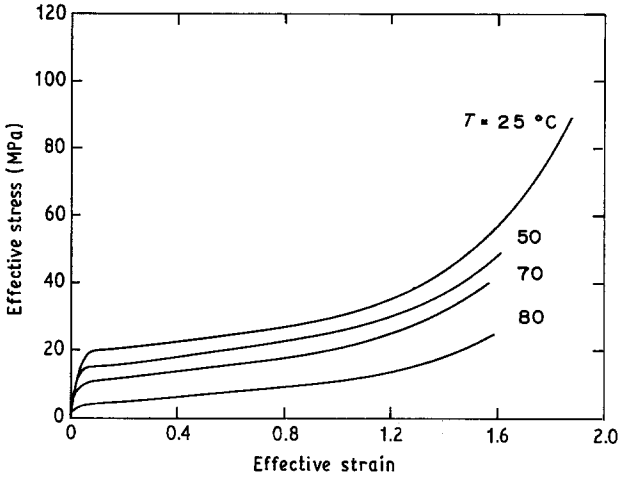

Figure 6 Influence of temperature on the effective stress–strain behaviour of high-density polyethylene at $\dot{\varepsilon}_{eff} = 1 \times 10^{-4}\ s^{-1}$.

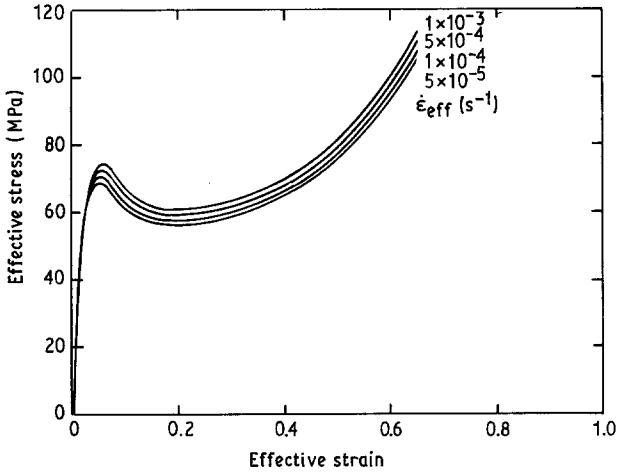

Figure 7 Effective stress–strain curves of polycarbonate at 25 °C for various strain rates.

here is not the effect of the cross-section reduction and corresponds necessarily to a true strain-softening of the polycarbonate. It was shown in a previous study [19] that this true yield drop is observed for all glassy polymers (thermoplastics and thermosets) below their glass-transition temperature. In polycarbonate, it makes the necking phenomenon particularly abrupt and unstable. In special instances (for example if the rigidity of the tensile grips is insufficient, or if the specimen is originally damaged) localized shear bands may develop at yield. For such situations, the video-controlled system provides the interesting advantage of giving in real time a dynamic view of the artefact, and lets the user decide on direct grounds whether the test should be discounted or not.

Once the transient yield stage is passed, it is noted (for effective strains larger than 0.2) that the continuation of the plastic flow proceeds with a gradually increasing strain-hardening, somewhat similar to the final stage of the polyethylene. Here the hardening would be caused by local rotation of the chain segments towards the direction of the tensile axis [20] and by a subsequent higher resistance to plastic deformation of this oriented amorphous structure.

The absolute shift between the curves of Fig. 7 obtained at different strain rates is somewhat lower than for the polyethylene. Furthermore, if computed as the relative variation of the tensile stress, the strain-rate sensitivity of polycarbonate is about three times less than for polyethylene.

Also, the tensile behaviour of the polycarbonate is very sensitive to the testing temperature as shown in Fig. 8. It should be noted in particular that the stress decreases very abruptly while approaching the glass transition temperature at $T_g = 145\,°C$. Above this temperature, the material becomes rubber-like and the yield stress approaches zero. As far as strain-hardening is concerned, it decreases rapidly between 100 °C and T_g but does not vanish completely in the rubbery state, since the polymer chains continue to be subjected to the entropic stress between the physical entanglements [21].

Particular attention should be paid to the shape of the yield drop at elevated temperatures (Fig. 9). Not only is the stress peak observed to become narrower when approaching the glass transition, but also its amplitude depends much more on the strain rate than it does at room temperature. It is remarkable how the peak is reduced at lower strain rates and eventually

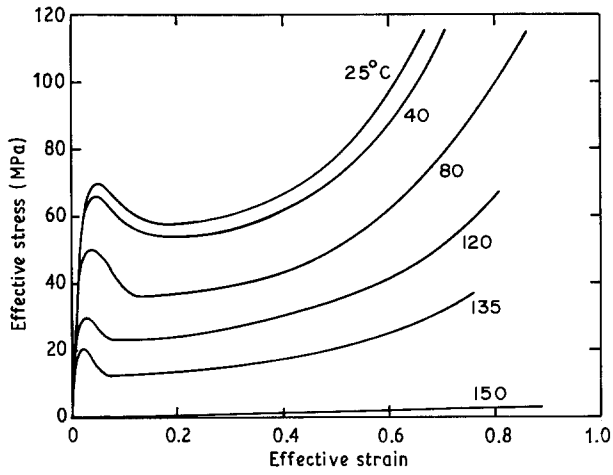

Figure 8 Influence of temperature on the effective stress–strain behaviour of polycarbonate at $\dot{\varepsilon}_{eff} = 1 \times 10^{-4}\ s^{-1}$.

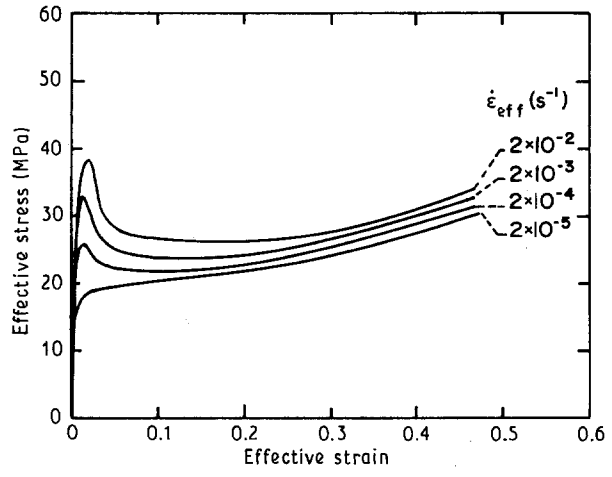

Figure 9 Influence of the effective strain rate on the yield drop of polycarbonate at 125 °C.

disappears at 10^{-5} s^{-1}.According to a previous model [22] this phenomenon would correspond to the unstable generation of deformation defects occurring at yield in the glassy polycarbonate. After the exhaustion of the available relaxation sites in the inelastic range, the irreversible plastic deformation would be initiated by the multiplication and growth of microscopic shear domains inclined to the tensile axis. The kinetics of this yielding process was described in a similar scheme as the transient plasticity model of Gilman and Johnston [23], originally introduced for inorganic materials. For appropriate values of the defect mobility and of the strain rate, the model predicts very large amplitude variations of the yield peak, quite like what is observed here.

3.3. Other materials

In order to assess its applicability, we have tested the above method with a number of other materials which are listed in Table I. The corresponding effective stress–strain curves are displayed in Fig. 10 and 11 for various polymers and metals tested at 25 °C. Also shown in Fig. 12 are the results for three polymers which were too brittle at the ambient temperature and

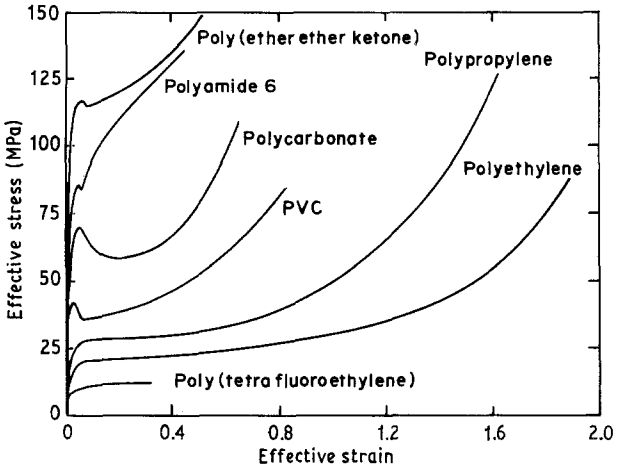

Figure 10 Typical effective stress–strain curves of seven ductile polymers at 25 °C and $\dot{\varepsilon}_{eff} = 1 \times 10^{-4}$ s^{-1}.

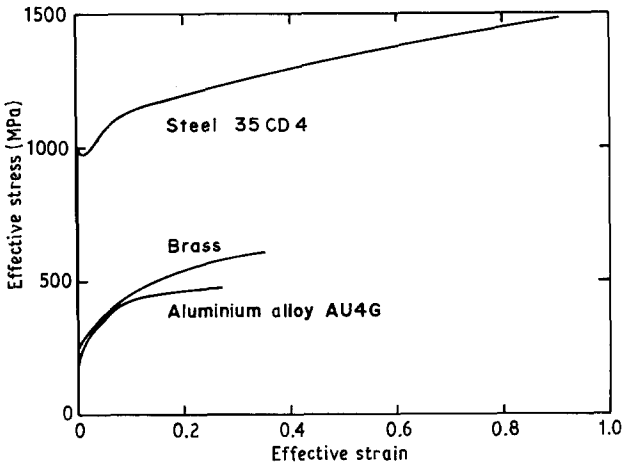

Figure 11 Typical effective stress–strain curves of three ductile metals at 25 °C and $\dot{\varepsilon}_{eff} = 1 \times 10^{-4}$ s^{-1}.

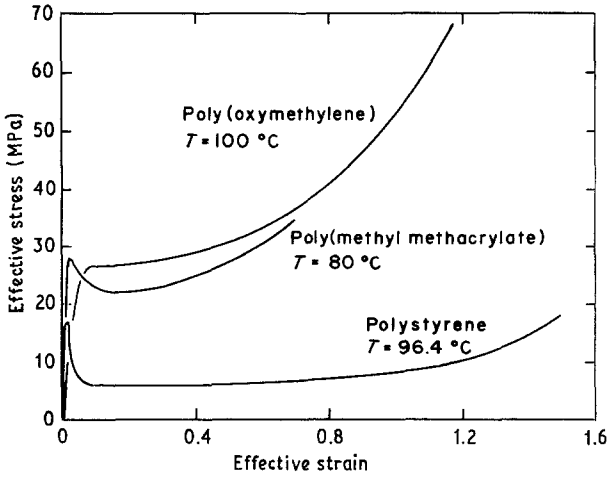

Figure 12 Typical effective stress–strain curves of three polymers at elevated temperatures; $\dot{\varepsilon}_{eff} = 1 \times 10^{-4}$ s^{-1}.

therefore investigated at a higher temperature. From these tests, it should be noted that

(i) the metallic materials (steel, brass, aluminium alloy) exhibit a plastic regime with a saturating strain-hardening, so that the necks continue to grow until rupture occurs;

(ii) the glassy polymers (PC, PS, PMMA, PVC) show a marked yield drop followed by a rapidly increasing strain hardening;

(iii) the semi-crystalline polymers tested below their glass-transition temperature (PA6, PEEK) yield with a very small stress peak since only their amorphous fraction is concerned in the defect generation mechanism and also because the crystallites act as favourable nucleation sites for the plastic mechanisms;

(iv) the semi-crystalline polymers tested above T_g (PE, PP, PTFE, POM) all have a very progressive elastic limit without any softening effect. This is because the interlamellar rubbery phase is flexible enough to accommodate the imposed strain rate before the crystalline chain slip mechanism can take over.

It should be remarked that the present testing technique allows the material to attain true strains at least equal to and often much larger than those in a conventional tensile test. In particular, the early fracture which is often encountered at the root of the gripped heads in the standard test-pieces is avoided in the hour-glass-shaped specimens for which the stress concentrations are considerably reduced.

4. Discussion

After having illustrated the applicability of the present testing method to a variety of materials, let us examine now in some details its specific capabilities, limitations and potential variants.

Originally, one of the authors [6] had initiated the analysis of the local plastic response of polymers with a view to giving a quantitative interpretation of the initiation and propagation of tensile instabilities. Several papers [3, 4, 7, 8] have shown that the effective stress–strain–strain-rate behaviour thus determined contains all the information necessary to predict the

kinetics of neck formation and growth in most types of stretching geometry.

Furthermore, it is clear from recent studies [24, 25] that the detailed shape of the effective stress–strain curves is a valuable indicator of the microstructural transformations of the material under stress. In the case of the semi-crystalline polyethylene, for example, the tensile behaviour at large strains reflects the complex evolution of the lamellar crystallites toward a fibre-like texture, as deformation proceeds. Consequently, comparing the shapes of the complete stress–strain curves for different materials is much more informative about their plastic mechanisms than simply comparing their yield stress and elongation at rupture.

In the course of assessing the performances of a material in relation to its structure, it is important to characterize the respective influence of strain and strain-rate on the tensile stress by mathematical equations. Since the present method gives access to the effect of each variable separately, the direct modelling of the experimental curves can be readily obtained. For example, it was shown [6] that the tensile behaviour of semi-crystalline polymers tested above T_g was closely described by a constitutive equation of the type

$$\sigma_{eff}(\varepsilon_{eff}, \dot{\varepsilon}_{eff}) = K[1 - \exp(-w\varepsilon_{eff})]\exp(h\varepsilon_{eff}^2)(\dot{\varepsilon}_{eff})^m \quad (8)$$

where the four parameters K, w, h and m depend on temperature. In terms of Eyring's process rate analysis [26] the strain-rate sensitivity coefficient, m, can be rewritten as indicated by

$$m = \left(\frac{\partial(\log \sigma_{eff})}{\partial(\log \dot{\varepsilon}_{eff})}\right)_{\varepsilon_{eff},T} = \frac{1}{\sigma_{eff}}\left(\frac{\partial(\sigma_{eff})}{\partial(\log \dot{\varepsilon}_{eff})}\right)_{\varepsilon_{eff},T} = \frac{kT}{v_{exp}} \quad (9)$$

where v_{exp} is the "experimental activation volume" of the Eyring theory, which characterizes the amount of material affected by the elementary deformation mechanisms.

Among the technical limitations of the method, two of them deserve to be discussed in more detail: the resolution and the sampling rate. The former is directly controlled by the number of pixels in the digitized video images. With the camera presently used, the linear resolution is equal to 1/512, that is about 0.2%. This corresponds to a somewhat modest precision in the pre-yield stage, but becomes very comfortable at large strains in the plastic regime. Cameras with 1024×1024 pixels have been developed recently, but their price is still high and the processing of their image is four times longer. The latter consideration opens the discussion towards the problem of speed. With commercial video cameras, the standard sampling rate is of 25 frames per second and the image digitization is operated within one frame only. Therefore there is no loss of time at this step. However, the digital treatments leading to the determination of the minimum diameter and the radius of curvature of the specimen are time-consuming, as well as the acquisition of the tensile force, the computation of the stress and strain, the control of the ram position and the plotting of the curves on the monitor. With all these additional software operations, the overall time required per frame is equal to about 0.1 s. Consequently, the method is presently restricted to tests run at strain rates not higher than $\dot{\varepsilon}_{eff} = 10^{-2}\,s^{-1}$. This could appear as a drastic limitation. However, a deeper analysis showed in the case of various polymers [9] that the material-imposed limit is even slower than this instrument-imposed limit if one wished to ensure strictly isothermal deformation of the sample. It was demonstrated, actually, that self-heating of polymers under irreversible plastic deformation is no longer compensated by heat conduction and convection losses for strain rates higher than about $3 \times 10^{-3}\,s^{-1}$, and consequently that faster strain rates should be avoided.

Another limitation arises from the assumption of isochoric deformation which has been adopted *ab initio* for deducing the axial component ε_{zz} from the radial component ε_{rr}. Although the $\varepsilon_{zz} = -2\varepsilon_{rr}$ equation is well verified in a large range of plastic strains for ductile materials, it is clear that the specimen volume may increase under tension: (i) when the deformation is elastic since the Poisson's ratio is then usually between 0.3 and 0.4 [6], (ii) in semi-crystalline polymers when crystallites are fragmented under stress [17], and (iii) when crazing or cavitation occurs under the effect of the negative hydrostatic pressure [27]. Conversely, the volume experiences a slight decrease in ductile amorphous polymers when the macromolecular chains rotate under strain towards the tensile axis [20]. Fortunately these effects are generally limited to a few per cent, so that the relative error for large plastic strains is negligible. Furthermore, if a model for the volume dilatation or contraction with strain (or stress) is available, it might be readily implemented within the control software, so that a more accurate expression for the effective strain could thus be taken into account.

In regard to the above minor limitations, the present method offers a very large field of possible applications, upgradings and variants. Among these advantages is the potentiality to adapt the system very easily to many other types of deformation geometry or schedule. We have successfully tested in this laboratory the case of simple shear tests [22]. Although it is not the object of this paper to describe this alternative testing procedure, it is interesting to remark that switching from tension control to shear control is only a question of minutes, since the hardware utilized in both methods is the same. For simple shear, the software which was developed (named VideoShear) measures in real time the local true shear strain by analysing the progressive distortion of a serigraphic ink marker printed on the flat surface of the specially designed shear specimens. As for tension tests, the local shear rate is kept constant by adequate control of the hydraulic ram speed.

Among the other applications of the video-controlled materials testing technique which are now in course of development in this laboratory, the following ones are of particular potential. As a direct exten-

sion of the tensile tests, a new procedure was designed for compression tests in order to take into account the so-called barrelling effect which arises as soon as the friction between the sample heads and the compression tools is significant. In this application (named VideoCompression), the video camera monitors the maximum diameter of the specimen in the mid-plane of the barrel, together with the local radius of curvature of the sample profile. From these data, a Bridgman-type stress triaxiality factor is computed to derive the effective stress–strain relation and the local compression strain-rate is held constant. Another type of test is presently being developed (VideoCreep) for performing creep tests at constant true stress. This system aims to investigate the ultimate creep stage in ductile polymers. In conventional creep tests performed at constant load, this stage is difficult to characterize since it corresponds to the catastrophic development of a neck in the sample. With the closed-loop video system, the load is reduced in real time in such a way that the local stress remains constant in the incipient neck, automatically. Last of these applications, a new system has been designed (named VideoFatigue) for the control of fatigue tests with standard compact tension (CT) specimens. In this procedure, the slow propagation of the fatigue crack is monitored with the camera every five periods and the load is controlled in real time in order to get a constant stress intensity factor, K_I. The exploitation of these new methods is in progress for specific materials and the results of the experiments will be the object of forthcoming publications.

5. Conclusions

A novel tensile testing method was developed for the determination of the plastic behaviour of ductile materials up to very large plastic strains. It is based on a digital video extensometer and on the real-time control of the local effective strain rate in the centre of an hour-glass-shaped test-piece. It was applied to various ductile polymeric and metallic materials. It was thus shown that

(i) the effective stress–strain–strain-rate constitutive equations are readily attained in real time without any need for data post-processing;

(ii) the yield behaviour and the large-strain plastic stage provide complementary information on the microscopic mechanisms of plastic deformation;

(iii) the present performances of the system (512×512 pixels, 100 ms frame processing time) constitute a reasonable optimum with respect to the present state of the technology and to the self-constraints of polymeric materials.

Acknowledgements

The development of this method was made possible thanks to the financial support of the DRET (French Ministry of National Defence). The authors are grateful to Mrs Gallicher, Engineer at the DRET, for continuous interest in this work.

References

1. R. M. McMECKING and J. R. RICE, *Int. J. Solids Struct.* **11** (1975) 601.
2. D. PIERCE, R. J. ASARO and A. NEEDLEMAN, *Acta Metall.* **31** (1983) 1960.
3. C. G'SELL, A. MARQUEZ-LUCERO, P. GILORMINI and J. J. JONAS, *ibid.* **33** (1985) 759.
4. C. G'SELL, A. MARQUEZ-LUCERO, A. SOUAHI and Y. S. TONG, in "Plastic Instabilities" (Presses des Ponts et Chaussées, Paris, 1985) p. 165.
5. P. S. HOPE, I. M. WARD and A. G. GIBSON, *J. Mater. Sci.* **15** (1980) 2207.
6. C. G'SELL and J. J. JONAS, *ibid.* **14** (1979) 583.
7. C. G'SELL, N. A. ALY-HELAL and J. J. JONAS, *ibid.* **18** (1983) 1731.
8. C. G'SELL, *Rev. Phys. Appl.* **23** (1988) 1095.
9. A. MARQUEZ-LUCERO, C. G'SELL and K. W. NEALE, *Polymer* **30** (1989) 636.
10. P. W. BRIDGMAN, *Trans. Amer. Soc. Metals* **32** (1944) 553.
11. R. J. ASARO, *Adv. Appl. Mech.* **23** (1983) 89.
12. J. W. HUTCHINSON and H. OBRECHT, *Fracture* **1** (1977) 101.
13. A. K. GHOSH, *Metall. Trans.*, **8A** (1977) 1221.
14. B. WUNDERLICH, "Macromolecular Physics", Vol. 1 (Academic, New York, 1973) pp. 97 and 338.
15. C. G'SELL and A. J. GOPEZ, *J. Mater. Sci.* **20** (1985) 3462.
16. P. B. BOWDEN and R. J. YOUNG, *ibid.* **9** (1974) 2034.
17. J. M. HAUDIN, in "Plastic Deformation of Amorphous and Semi-Crystalline Materials", edited by B. Escaig and C. G'Sell, (Editions de Physique, Les Ulis, 1982) p. 291.
18. A. PETERLIN, *J. Mater. Sci.* **6** (1971) 490.
19. C. G'SELL and J. J. JONAS, *ibid.* **16** (1981) 1956.
20. D. J. BROWN and A. H. WINDLE, *ibid.* **19** (1984) 1997.
21. Y. TERMONIA and D. J. WALSH, *ibid.* **24** (1989) 247.
22. C. G'SELL, in "Strength of Metals and Alloys", edited by H. J. McQueen, J. P. Bailon, J. J. Dickson, J. J. Jonas and M. F. Arkben (Pergamon, Oxford, UK, 1986) p. 1943.
23. W. G. JOHNSTON, *J. Appl. Phys.* **33** (1962) 2716.
24. S. AHZI, D. PARKS and A. ARGON, *Polym. Prep.* **30** (1989) 55.
25. A. DAHOUN, C. G'SELL, G. R. CANOVA, A.MOLINARI and M. J. PHILIPPE, in Proceedings of International Conference on the Textures of Materials (ICOTOM 9), Avignon, September 1990, in press.
26. H. EYRING, *J. Chem. Phys.* **4** (1936) 283.
27. O. FRANK and J. LEHMANN, *Colloid Polym. Sci.* **264** (1986) 473.

Received 20 May
and accepted 27 September 1991